Analyzing Fluxional Molecules using DORI

Laurent Vannay,[a] Benjamin Meyer,[a] Riccardo Petraglia,[a][c] Giuseppe Sforazzini,[b] Michele Ceriotti[c][d] and Clémence Corminboeuf[a][d]*

[a]Laboratory for Computational Molecular Design, Ecole Polytechnique Fédérale de Lausanne, CH-1015 Lausanne, Switzerland

[b]Laboratory of Macromolecular and Organic Materials, Institute of Material Science and Engineering, Ecole Polytechnique Fédérale de Lausanne, 1015 Lausanne, Switzerland

[c]Laboratory of Computational Science and Modeling, Institute of Materials, Ecole Polytechnique Fédérale de Lausanne, 1015 Lausanne, Switzerland

[d]National Center for Computational Design and Discovery of Novel Materials (MARVEL), Ecole Polytechnique Fédérale de Lausanne (EPFL), 1015 Lausanne, Switzerland

Address correspondence to: clemence.corminboeuf@epfl.ch

ABSTRACT

The Density Overlap Region Indicator (DORI) is a density-based scalar field that reveals covalent bonding patterns and non-covalent interactions in the same value range. This work goes beyond the traditional static quantum chemistry use of scalar fields and illustrates the suitability of DORI for analyzing geometrical and electronic signatures in highly fluxional molecular systems. Examples include a dithiocyclophane, which possesses multiple local minima with differing extents of π-stacking interactions and a temperature dependent rotation of a molecular rotor, where the descriptor is employed to capture fingerprints of CH-π and π-π interactions. Finally, DORI serves to examine the fluctuating π-conjugation pathway of a photochromic torsional switch (PTS). Attention is also placed on post-processing the large amount of generated data and juxtaposing DORI with a data-driven low-dimensional representation of the structural landscape.

INTRODUCTION

Quantum chemical approaches generally rely upon the wavefunction or the electron density, which are both intricate and difficult to interpret. The wavefunction is undeniably a complex multidimensional object, while the electron density is rather featureless.[1–8] One way of overcoming this *conundrum* is to use molecular scalar fields, which condense the chemically relevant information obtained from quantum calculations into one single intuitive real space function (see Figure 1).

One of the most illustrative molecular scalar field is certainly the Electron Localization Function (ELF),[9–11] which identifies regions where electrons locate[1] and classify chemical bonds.[3] Different localization measures such as the Localized Orbital Locator (LOL),[12] the Parity Function (*P*),[13,14] the Electron Pair Localization Function (EPLF),[15] the Localized Electron Detector (LED),[16] the Electron Localizability Indicator (ELI)[17] or the single exponential decay detector (SEDD) have reinforced the interpretative power of scalar fields, while also extending their range of applications to post-Hartree-Fock (*e.g.*, ELI),[18] quantum Monte Carlo (*e.g.*, EPLF)[19] and orbital free formalisms (*e.g.*, LED, SEDD).

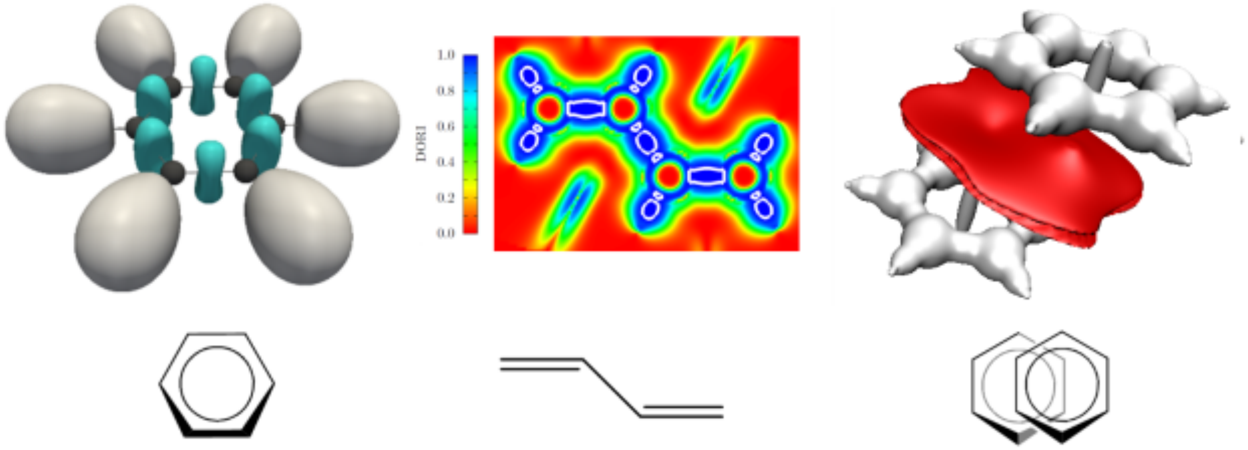

Figure 1: Three-dimensional representation of the benzene plotted for ELF= 0.8 (left), two-dimensional DORI maps in the σ_h plane of the butadiene with DORI=0.99 isocontour in white (center) and three-dimensional representation of the parallel-displaced benzene dimer for DORI=0.95 (right) with the covalent/non-covalent DORI domains in white/red respectively. Electron densities are self-consistently optimized at the B3LYP/TZP level.

The aforementioned scalar fields identify regions where electrons locate, which by design, precludes their identification of non-covalent regions where electrons are not well localized. The Non Covalent Interaction (NCI)[20] method was developed to fill this gap by specifically highlighting regions of low electron density gradient and low densities. Other approaches revealing covalent bonding patterns and non-covalent interactions simultaneously are also available, either through coupling different scalar fields (*e.g.* ELF and NCI)[21,22] or through stand-alone methods like the versatile Quantum Theory of Atoms and Molecules (QTAIM).[23–26] This work exploits another powerful scalar field, the Density Overlap Region Indicator (DORI),[27] introduced by de Silva and Corminboeuf, which was derived from the single exponential decay detector.[28–30] In short, DORI captures regions of space where the electron density between atoms, molecules or atomic shells clash. Such regions are characteristic of covalent and non-covalent interactions, both of which are revealed by DORI in the same value range. The scalar field probes geometrical features of the electron density in these overlapping regions by measuring the deviation from a single-exponential decay. The descriptor is dimensionless and solely dependent upon the electron density and its derivatives (eq. 1):

$$\mathrm{DORI}[\rho(\boldsymbol{r})] = \frac{\theta[\rho(\boldsymbol{r})]}{1+\theta[\rho(\boldsymbol{r})]} \qquad (1)$$

where

$$\theta[\rho(\boldsymbol{r})] = \frac{\left(\nabla\left(\frac{\nabla\rho(\boldsymbol{r})}{\rho(\boldsymbol{r})}\right)^{2}\right)^{2}}{\left(\frac{\nabla\rho(\boldsymbol{r})}{\rho(\boldsymbol{r})}\right)^{6}} \qquad (2)$$

Thus, DORI is well defined at any level of theory, and can also be exploited with orbital-free approaches as well as proatomic and experimental densities.[31] It is worth noting that a physical interpretation of DORI has been provided in terms of the local wavevector,[32–34] which reflects the shape of the electron density.

Molecular scalar fields have generally proved to be both insightful and reliable in a comprehensive range of applications. They can distinguish between different classes of chemical bonds[35,36] including metal-metal,[37,38] metal-ligand,[39,40] organic,[41–46] ionic,[47] or multicenter.[48] Moreover, they also reveal non-bonding interactions such as *e.g.* hydrogen[49–51] or halogen bonds[52–55] and vdW interactions in the excited state and have helped rationalize chemical reactivity involving *e.g.* cycloaddition,[56] hydrogen transfer,[57] or electron transfer[58] mechanisms, in systems ranging from organic[59–62] to metallic.[63,64] The range of DORI applications is comparably broad and includes: the construction of different classes of exchange-correlation functionals[65,66] and adaptive QM/MM schemes,[67] the characterization of nanomaterials,[68] the classification of excited states,[69,70] the identification of fingerprints associated with CO_2 sequestration by organic molecules,[71] and the conformational behavior of small bio-organic molecules[46] and hydrogen-hydrogen contacts in zincocene related compounds.[45]

Each of the aforementioned applications essentially rely upon a traditional “static” quantum chemistry picture, in which only one or a handful of gas phase 0K structures are considered. Yet, aside from a few cases involving small and rigid molecules, static representations of chemical processes may not provide a comprehensive picture. Indeed, there are many interesting phenomena that involve highly fluxional molecules where thermal motion heavily influence molecular properties. Examples include the subtle relative energy prediction of polymorphic crystal structures of floppy molecules,[72] the world of molecular actuators[73–79] as well as organocatalytic processes,[72] each of which all evolve on complex potential energy surfaces. For these types of systems, static descriptions are insufficient[80] and molecular dynamic (MD) trajectories become necessary. Of course, fluxional processes could still benefit from insights provided by molecular scalar fields as has been occasionally shown. One relevant example is Bonding Evolution Theory (BET),[81,82] which is a combination of ELF and catastrophe theory,[83] and can be used to discriminate specific events during a reaction processes (*e.g.,* bond formation or dissociation). Given the importance of non-covalent interactions an ELF/NCI cross interpretative BET strategy was also recently employed to monitor the full range of interactions.[21] While BET does add significant insight into chemical reaction,[60,84,85] its applications have been constrained to intrinsic reaction coordinates, which facilitate easy understanding of reaction mechanisms, but does not necessarily reflect dynamical processes. As mentioned by Piquemal[21] BET is, in principle, applicable to MD trajectories, but this possibility awaits further exploration.

The averaged NCI index (aNCI),[86] an extension of the existing NCI framework, is another strategy, which accounts for the fluctuation of the environment around a target molecule. Within aNCI, the environment is allowed to fluctuate while the geometry of the solute molecule is kept frozen. As such, aNCI effectively samples the solute-solvent fluxional interactions for a given solute geometry, but is unable to describe the inherent fluxionality of a solute molecule.

The only example exploring the effects of dynamical fluctuations on ELF and QTAIM was a prototypical SN_2 reaction by Adamo and co-workers.[87] In this work, the "crucial role of the electron charge transfers during the formation of the ion−dipole complex"[87] was only properly described using dynamical analysis. Still, the system investigated (chlorine exchange in chloroform) had a limited number of degrees of freedom. Along a similar line, the pioneering ELF investigation of Marx and Savin,[88] on the elusive bonding of the "highly fluxional" CH_5^+ molecule should be mentioned. The authors analyzed a "statistical sample" of 64 molecules extracted from an MD trajectory to clearly distinguish between the three-center, two-electron H_2-C bond, from the remaining three two-center, two-electron CH bonds.

This number of examples present in the literature already illustrates the suitability of using bonding descriptors beyond traditional static quantum chemical situations. This work goes a step further and demonstrate the usefulness of DORI[27] to analyze covalent bonding patterns and non-covalent interactions in three highly fluxional systems (Figure 2).

The first example is a dithiocyclophane (**1**)[89–91] that is dominated by low energy conformations characterized by different extent of intramolecuar π-stacking that are well described by DORI. For the molecular rotor (**2**),[91,92] DORI is used to fingerprint and discriminate between the compact enthalpy-driven structures and the disordered conformations. Finally, DORI is used to examine the fluctuating π-conjugation pathway of a photochromic torsional switch (PTS, **3**).[93] We stress that the objective of this work is to emphasize the usefulness of a density-based property, such as DORI, to discriminate between covalent and non-covalent interaction patterns in highly flexible molecules and not to invoke any possible correlation between DORI and interaction energies.

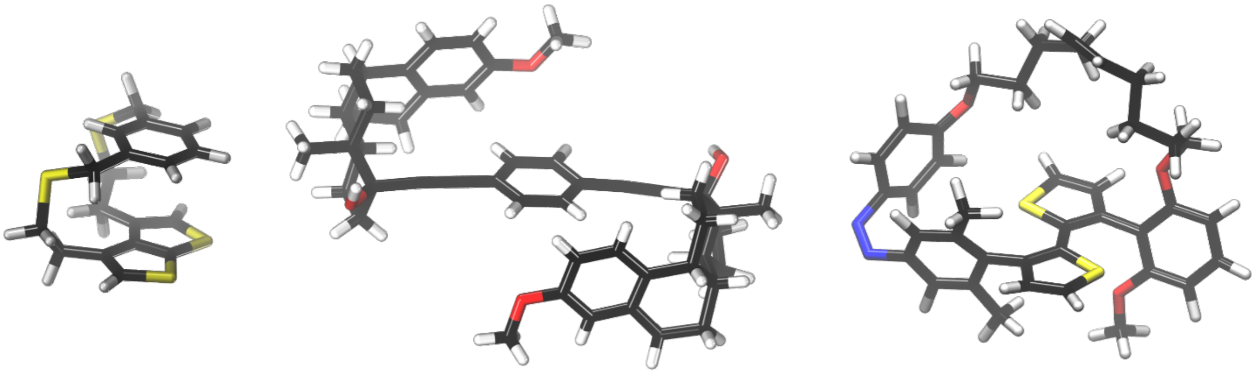

(1) (2) (3)

Figure 2: 3D representation of Thieno-[2,3-b]-thiophene (**1**), a molecular rotor (**2**) and a photochromic torsional switch (**3**).

COMPUTATIONAL DETAILS

Molecular dynamics trajectories of **1-3** were performed using Born-Oppenheimer MD (BOMD) at the DFTB3 level,[94–96] as well as our recent REMD@DFTB3 variant[91] that combines Density Functional Tight Binding (DFTB3) in DFTB^{+} [97] with Replica Exchange Molecular Dynamics (REMD, parallel tempering) powered by i-PI.[98,99]

REMD performs several molecular dynamic trajectories (*i.e.,* replica) at different temperature with each replica being able to exchange its atomic positions and velocities each of the other replicas. The algorithm dictating the exchange keeps all the replicas in the respective canonical ensemble for the targeted temperature. For **1** and **2**, the trajectories were taken directly from reference 91, while for **3** trajectories are based on from reference 93. We analyzed the gas phase trajectories at 300K for **1** and **3**, and at 310K for **2**.

The BOMD trajectories of **1** ran for 5.4x10^6 steps assembled from 54 equivalent simulations initiated with random configurations generated from previous BOMD. REMD temperature ranges from 300K to 1500K with 16 replicas (2x10^5 steps/replica) for **1**, and 48 replicas (1.5x10^5 steps/replica) for **2**. A Langevin thermostat with a time constant of 100 fs kept each replica at a constant temperature. For (**3**), the REMD temperature ranged from 300K to 1200K using 32 replicas (1.5x10^5 steps/replica), and a GLE thermostat[100] to improve the mapping. For all three systems, a time step of 0.25 fs was found to be sufficient to avoid any drift in the conserved quantity while integrating the Newton equations. All forces were computed at the DFTB3/3OB[101,102] level, with the dispersion correction based on the Universal Force Field parameters[103] as implemented in the DFTB+ code.[97]

The REMD@DFTB3 trajectories at the targeted temperature are then post-processed exploiting DORI. All electron densities used for DORI were computed at the PBE/6-31G* level in Gaussian09 on a subset of random snapshots extracted from the REMD or MD trajectories.

The quantitative analysis was performed by integrating the electron density or considering the volume associated with the relevant DORI domains defined by a given DORI isovalue (V_{iso}):

$$DORI_{int}[V_{iso}] = \int_{V_{iso}} \rho(r)dr \qquad (3)$$

$$DORI_{vol}[V_{iso}] = \int_{V_{iso}} dr \qquad (4)$$

Both $DORI_{vol}$ (in Bohr^3) and $DORI_{int}$ (in electron/Bohr^3) capture the relevant bonding or non-covalent patterns and are capable of distinguishing between the signatures of rather directional H-bonds (smaller DORI basin volume) and more diffuse π-stacking interactions (larger DORI basin volume) characterizing the different molecular conformers (see Figure S1 and S2 the in Supporting Information). Here, $DORI_{vol}$ is favored for the evaluation of non-covalent interactions, whereas the integration of the density is more intuitive when discussing a covalent bonding pattern. For all systems, DORI, $DORI_{int}$ and $DORI_{vol}$ were computed on a locally modified version of DGRID-4.6, with a precision of at least 10points/Bohr. The isovalue taken for each system was chosen such as the basin representative of the targeted interaction remains separated from the other domains. As discussed in the original DORI paper,[27] the quantitative analyses are thus dependent upon the chosen isovalue. We insure that the trends persist for any selected isovalue leading to similar domain separations (see Figures S1, S3 and S4 in the SI). In the case of the dithiacyclophane (**1**) and rotor (**2**), the $DORI_{int}$ and $DORI_{vol}$ were computed on a truncated frozen snapshot geometries saturated with hydrogen atoms, placing emphasis on the targeted interaction. While not mandatory, such a truncation accelerates the DORI analysis without modifying the relevant contributions to the targeted domains (see Figure S5 and a detailed description in the SI).

The π-conjugation pattern within the dithiophene unit of the photochromic torsional switch[93] was analyzed using DORIπ, corresponding to the DORI function based on the π-density only. The relevant orbitals (see Figure S6 in the SI) were localized using the Adaptive Natural Density Partitioning (AdNDP) proposed by Boldyrev and co-workers,[104–106] which is ideally suited for this purpose (see supplementary information for the detailed procedure).

Finally, the conformational spaces of the molecular rotor and the photochromic torsional switch are depicted using the sketch-map dimensionality reduction algorithm[107–109] (see S.I. for the detailed procedure).

Results and Discussion

Thieno-[2,3-b]-thiophene

The π-stacked, arrangement of (hetero)aromatic cores is a distinct packing motif associated with pronounced optical and semiconducting properties.[110] Previously, DORI was shown to be a useful descriptor of the "electronic compactness" of π-stacked motifs in quatertiophene crystals[27] and one-dimensional nanofibrils.[68,80] In these materials, solubilizing side chains, hydrogen-bond and dispersion-driven aggregators were exploited to achieve tight packing, which was conveniently probed using the integration of the electron density within the DORI intermolecular domains (DORI_{int}) (*i.e.*, electronic compactness). The DORI-based “electronic compactness”[27] largely correlated with charge mobility albeit offering distinct information.[80]

Along the same line, the bridged asymmetrically polarized dithiacyclophane incorporating a thieno-[2,3-b]-thiophene[89] (**1**), possesses two low-lying π–π stacked conformers.[111] Thus, it is ideally suited for evaluating the advantages of DORI over geometrical variables for analyzing packing fluctuations. Two geometrical collective variables characterize this “molecular pac-man”: the distance between the center of mass of the rings and the angle between the normal to the plane formed by the atoms in the rings (Figure 3). The relation between the geometrical criteria and the DORI_{int} value of 10’000 snapshots extracted from 54 independent 25 ps NVT DFTB molecular dynamic trajectories (1.35 ns in total) at 300 K is presented in Figure 3. The “π-stacked conformational region” corresponds to small R and θ values where the density overlap, *i.e.*, DORI_{int}, is significant (red, orange). Inversely, DORI_{int} vanishes when the molecule opens (*i.e.* for large R and θ values) as the density overlap decrease toward zero (blue). Valuably, DORI encompasses all the structural and electronic features associated with the π-stacking pattern into a single (DORI_{int}) value. For instance, Figure 3 clearly shows that the density overlap is more sensitive to R than to θ.

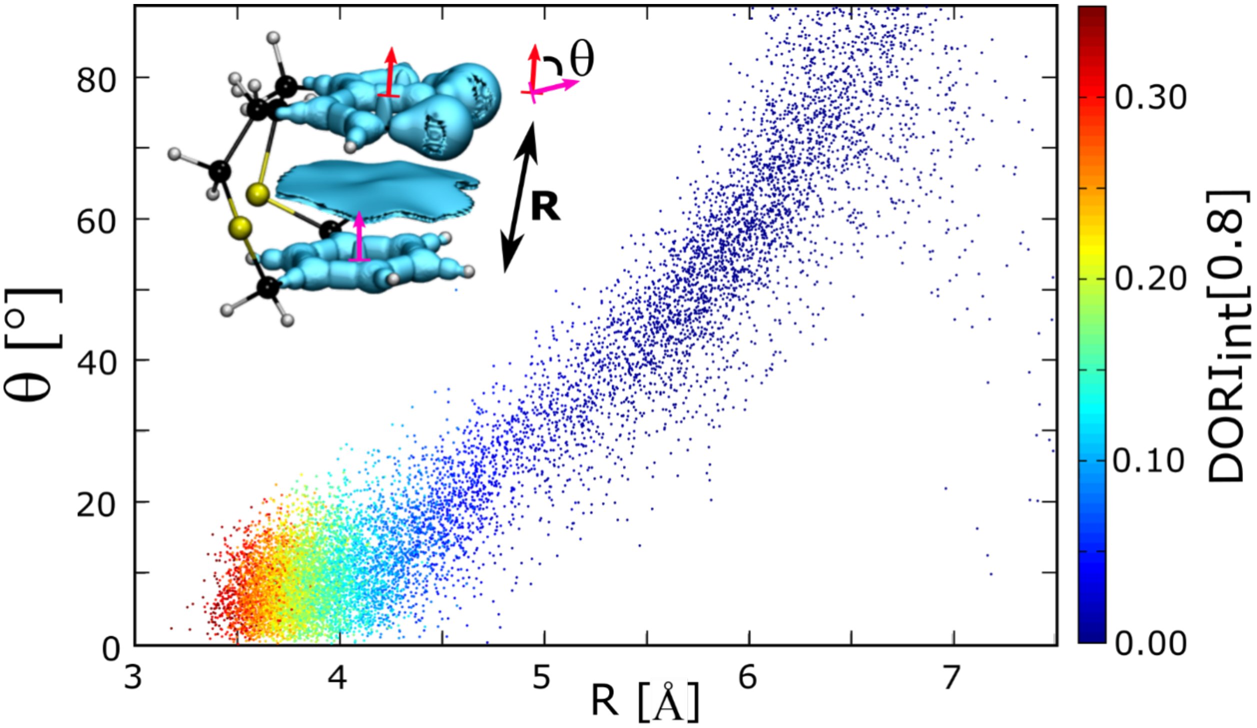

Figure 3: Two-dimensional representation of the dithiacycloplane conformers color-coded with the integral of the electron density within the intramolecular DORI domain, $\mathrm{DORI_{int}}[0.80]$ (in electron/Bohr^3). Conformers are extracted from DFTB trajectories at 300K. The snapshots are described based on the distance between the center of mass of the π-subsystems (R), and the angle between the two planes describing the π-systems (θ) mapped in the [0,90] range. DORI values are computed on electron densities relaxed at the PBE/6-31G* level on frozen DFTB3/3OB-UFF MD geometries.

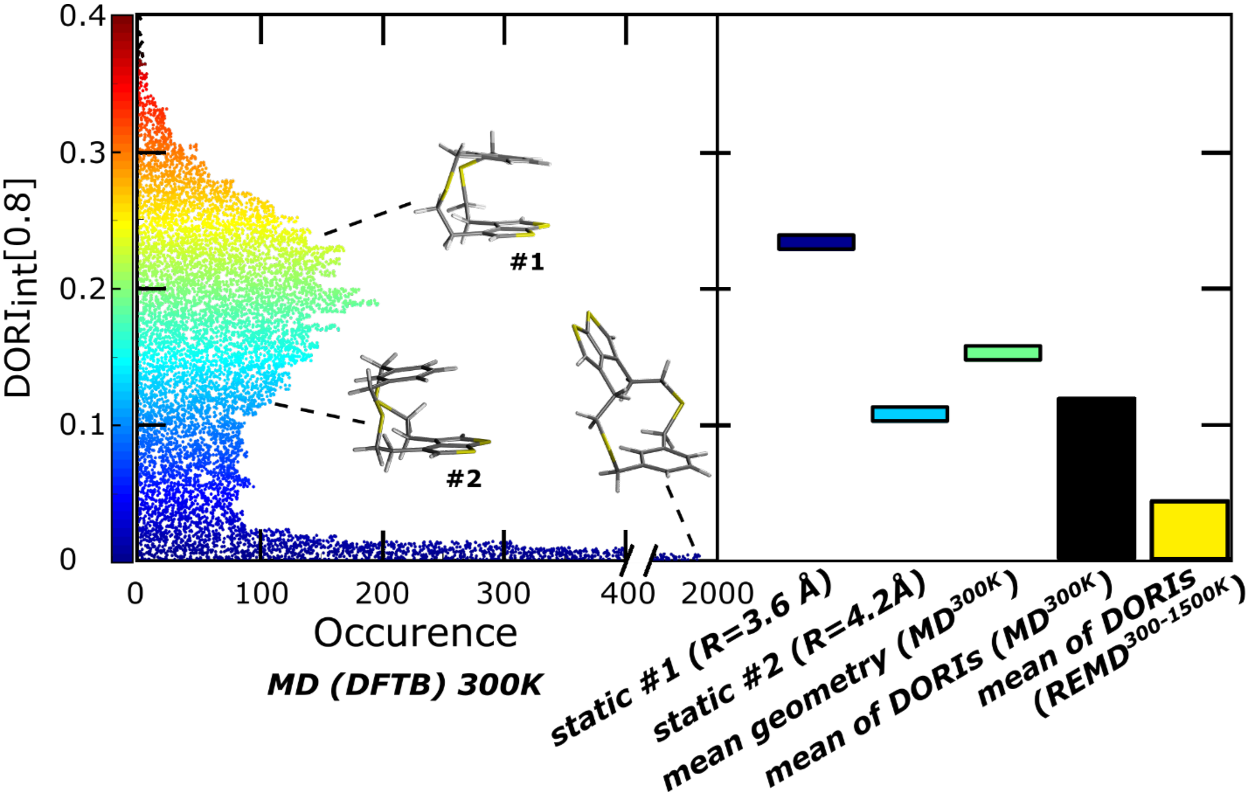

Figure 4: Structure occurrence based on integral of the electron density ($\mathrm{DORI}_{\mathrm{int}}$[0.8] in electron/Bohr^{3}) within the intramolecular DORI=0.8 domain of the truncated dithiocyclophane, computed on the structures extracted from the MD (left). $\mathrm{DORI}_{\mathrm{int}}$[0.8] of two optimized geometries (static **#1**, **#2**), the average MD geometry, and mean of DORIs from the standard MD at 300K, and from REMD@DFTB3^300K. DORI are computed on electron densities relaxed at the PBE/6-31G* level, on DFTB3/3OB-UFF (MD) geometries.

The comparison between the snapshots of the 300 K MD trajectories and the static gas phase geometry highlights the pronounced π-stacking fluctuations typical of this molecule. As mentioned earlier, two π-stacked minima having an interplane distance of 3.6 and 4.2Å were found by static optimizations at the DFTB (or DFT).[90] These minima are within 2 kcal mol^{-1} of one another (in favor of the former at the DFTB3/3OB level) and are associated with an electronic compactness, of 0.24 and 0.11 electrons, respectively (as measured by *i.e.* $\mathrm{DORI}_{\mathrm{int}}$[0.8], see Figure 4). According to the $\mathrm{DORI}_{\mathrm{int}}$ profile, the fluxional behavior of dithiacyclophane causes neither of the two static structures to be very representative of the molecule (see the time evolution of $\mathrm{DORI_{int}}$ in Figure S3 in supporting information). Within the timescale explored (1.35 ns), the molecule predominantly oscillates between these two conformations. Occasionally a third region represented by an open conformation is also visible. The ensemble of $\mathrm{DORI_{int}}$ values shows a Gaussian distribution centered between the two closed conformations ($\mathrm{DORI_{int}}=0.19$) but closer to the lower lying stacked minimum. A non-negligible contribution also arises from the open form ($\mathrm{DORI_{int}} < 0.05$). For this flexible system, it was demonstrated that only a more efficient sampling technique, *e.g.*, REMD@DFTB3, permits a thorough exploration of the potential energy surface and reveals the presence of another dominant conformational “disarticulated” region.[91] When the structures stemming from all three conformational regions are accounted for (*i.e.*, from REMD@DFTB3), the π-stacked conformations become less prevalent and the resulting mean $\mathrm{DORI_{int}}$ value is consequently much closer to zero. Taken together, this system clearly illustrates the importance of merging traditional quantum chemistry with accelerated sampling techniques prior to applying density-based descriptors that are capable of recognizing interaction patterns.

Molecular rotor

Molecular rotors are one of the most illustrative classes of fluxional systems. These molecules usually comprise a fairly static component (the stator) and a more flexible and eventually switchable unit (the rotator). One of the main computational and experimental challenge consists in understanding[112,113] and controlling[114,115] molecular flexibility and dynamic motion within the system such that more efficient rotors can be designed.[116] One key factor influencing the rotor dynamics is the torsional potential, which is highly sensitive to the nature and strength of the non-covalent interactions occurring between the rotator and the stator.[116] We illustrate this aspect by considering the dynamic motion of a recently synthesized molecular rotor (**2**), which features enthalpy driven conformational states stabilized by stator-rotor non-covalent interactions and more disordered (entropically favored) conformational states.[92] In this system, the subtle interplay between the enthalpy and entropic factors was evaluated experimentally using variable-temperature NMR,[92] and computationally by both a static[92] and an REMD@DFTB3[91] picture.

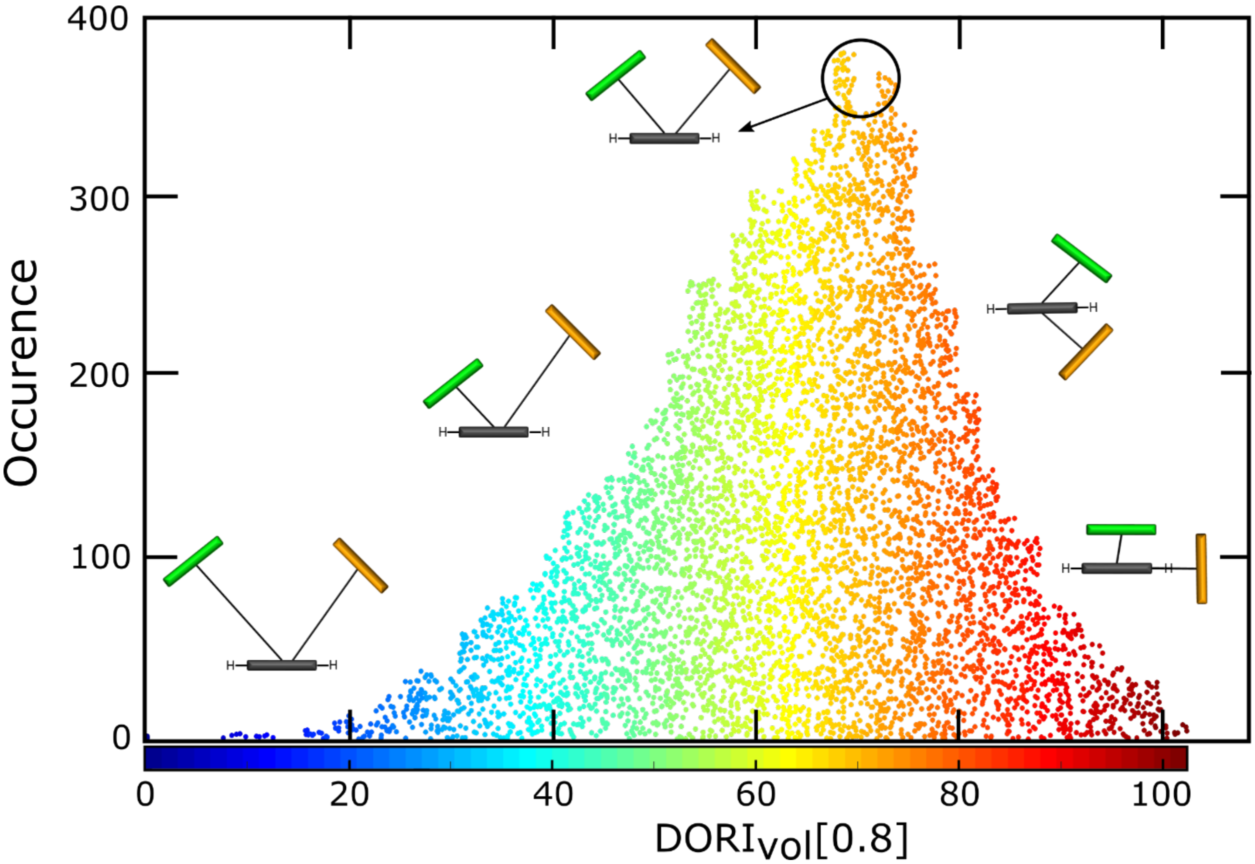

Figure 5: Schematic representations of the molecular rotor and their occurrence in function of their $\mathrm{DORI_{vol}}$[0.8] in $\mathrm{Bohr^3}$. The histogram is equivalent to the barre histogram in Figure S1 (see SI) except that each point corresponding to a structure, with the x-value being its DORI volume, is represented. Within a given interval of 2.0 $\mathrm{Bohr^3}$, the y-value is randomly attributed (using a random uniform distribution function) to each point in the range [0,hist(y)], where hist(y) is the y-value of the histogram depicted in Figure S1.

$\mathrm{DORI_{vol}}$[0.8] values are computed on the model system using the DORI domains stemming from the two stator-rotator interactions. DORI are computed on electron densities relaxed at the PBE/6-31G* level on the DFTB3/3OB-UFF REMD geometries.

The structural motifs featuring the rotor and the stator throughout the fluxional process at 310 K are schematically represented in Figure 5. Conveniently, the individual structural patterns have specific DORI signatures, encoded by their unique non-covalent DORI domains. The characteristic volume of these domains, $\mathrm{DORI}_{\mathrm{vol}}$, can be monitored across the simulation to identify the dominant conformations. The histogram in Figure 5 displays the relative occurrence of each of these patterns sampled at 310 K (using REMD) in terms of $\mathrm{DORI}_{\mathrm{vol}}$. The figure uncovers the clear dominance of the disordered conformations. The patterns range from a small number of very open-structures ($\mathrm{DORI}_{\mathrm{vol}} \sim$ 0-30 bohr^3), where there is nearly no overlap between the rotor and the two stators, to the frequently visited and dominant disordered structures that feature loose π-π or CH-π contacts, visible for $\mathrm{DORI}_{\mathrm{vol}} < 70$ bohr^3. The largest $\mathrm{DORI}_{\mathrm{vol}}$ (between 80 and 100 bohr^3) are associated with the reduced assortment of very compact enthalpy-driven conformations, which possess substantial π-π or CH-π contacts. The predominance of the disordered (*i.e.*, entropy driven) conformations aligns well with experiment[92] and with our alternative analysis of the REMD@DFTB3 results[91] based on chemical shifts. Given the floppy nature of the systems discussed in this work, it is clear that many geometric parameters would be needed to fully characterize all of the different molecular fluctuations. DORI fingerprints, instead, provide a single value that captures the structural and electronic information of the different molecular conformers. In order to assess the extent to which this single parameter can characterize the complex structural landscape of fluxional molecules, it would be useful to juxtapose DORI with a data-driven low-dimensional representation of the structural landscape, rather than with few, more or less, arbitrarily selected collective variables. Fortunately, numerous algorithms have been developed for reducing the dimensionality of the representation of complex free-energy surfaces using linear (*e.g.*, principal component analysis[117–119]) and more elaborate non-linear projections (*e.g.*, ISOMAP,[120] Laplacian eigenmaps[121], locally linear embedding[122] or sketch-map[107–109]). Here, the sketch-map technique specifically introduced by Ceriotti *et al*. was used to analyze atomistic data characterized by high dimensional thermal fluctuations.[107,109]

Sketch-maps can be generated starting from any suitable high-dimensional representation of an atomistic configuration, and reduce this description to a low-dimensional (often, 2D) description in a way that preserves proximity between states: two points close on the sketch-maps share high structural resemblance in the high-dimensional space. Sketch-map has been successfully employed to describe the conformational space of proteins,[109,123] extended solids,[124] molecular and model clusters,[108,124] to bias MD simulations,[109] or to classify (high-throughput) structural databases.[124,125] In this work, in order to avoid any bias in the construction of the low-dimensional representation, we do not select specific high-dimensional descriptors, but use a general measure of structural similarity[124] that only relies on a combination of comparisons of local atomic environments. Owing to the highly flexible nature of the molecular rotor, **2**, no clear-cut free-energy basins emerge from the sketch-map analysis (see Figure 6). However, despite the breadth of the basin, structures with comparable interactions are projected close to each other in this representation. When the map is color-coded with $\mathrm{DORI}_{\mathrm{vol}}[0.8]$ values, it becomes clear that even without identifying separate structural clusters the sketch-map representation captures the essential features of the fluctuations of the rotor: a drift from high density overlap conformations (right, orange) to open forms of the rotor (left blue) is clearly visible. This observation demonstrates that sketch-map determines in an automatic, agnostic fashion structural features that are strongly connected with different levels of non-covalent bonding. Conversely, the excellent correlation between the main sketch-map variables and DORI prove that this density-based fingerprints can effectively capture the essential structural features of a highly fluxional system.

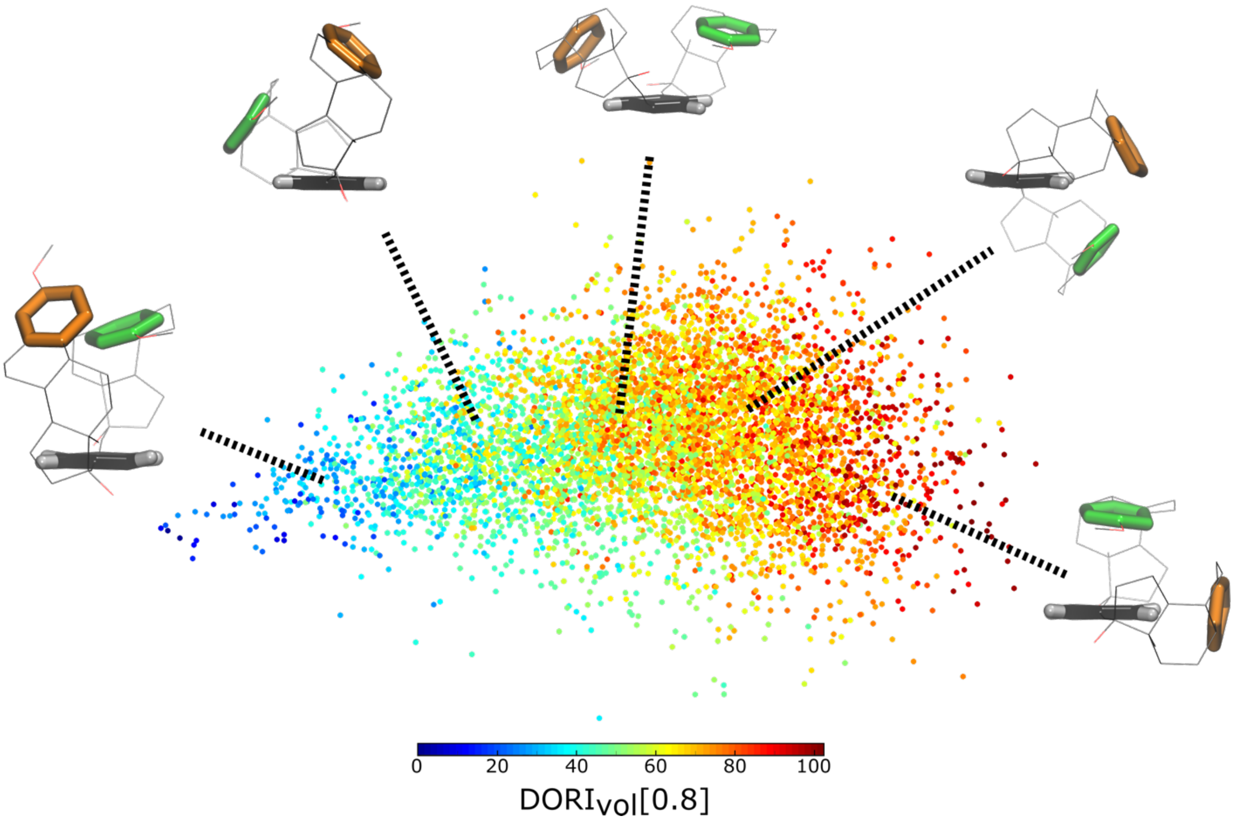

Figure 6: Sketch-map representation of the molecular rotor **2**, color-coded with the sum of the DORI$_{vol}$[0.8] (in Bohr^3) stemming from interactions between the two stators and the rotator.

Photochromic torsional switch

In the previous examples, DORI was used to characterize only non-covalent interactions. Considering that the descriptor also capably distinguishes different bonding patterns, the final example uses DORI to gauge the extent of π-conjugation in a photochromic torsional switch (PTS) comprised of a azobenzene and a bithiophene subunit.[93] In this PTS, a strong rearrangement upon photoisomerization modulates the π-conjugation within the bithiophene subunit.[93] In short, the *Z* azobenzene configuration allows the bithiophene subunit to achieve a quasi-planar anticonformation, whereas a twisted bithiophene dominates the *E* azobenzene configuration. This torsion-planarization, which directly impacts the extent of π-conjugation, was probed experimentally by measuring the absorption spectra.[93] Here, the conjugation strength is monitored by the DORIπ_{int} of the inter-thiophene bond in Figures 7 and 8. As evident from Figure 7 (right), neither the ∠SCCS dihedral angle (θ), nor the inter-thiophene carbon-carbon bond (R) entirely describes the extent of delocalization. Both the *Z* and *E* configurations are affected by thermal fluctuations meaning that for a given dihedral angle (θ) characteristic of the planar dithiophene (*i.e.*, Z-azobenzene configuration, inter-thiophene $\theta \in [120,180]$), the π-conjugation (*i.e.*, DORIπ_{int}) decreases as the bond length increases. Similarly, for a fixed C-C bond length, the DORIπ_{int} weakens as the two thiophenes twist out of planarity. Hence, DORIπ_{int} decreases when the π-delocalization is reduced either by bond lengthening and/or deplanarization of the dithiophene. The sketch-map in Figure 8, which clearly separates the *E* from the *Z*-azobenzene configurations without using arbitrarily selecting collective variables, is even more insightful when enriched by a color coding based on the DORIπ_{int} values. The rather weak π-conjugation (coinciding with low DORIπ_{int} values, light blue-green) is distinctive of the *E*-azobenzene configuration, which contrasts with the dominant red color (larger π-conjugation) of the *Z*-azobenzene region. While this difference attests that this switch efficiently modulates the extent of π-conjugation within the bithiophene unit, the electronic information encoded in this DORIπ_{int}-based map is more comprehensive than the geometrical variables as it captures both the imperfection of the switching design (*i.e.,* the switch is not perfectly forcing the bithiophene unit out of planarity in its E configuration or planarity in the Z configuration) and the softness of the inter-thiophene all reflected by the green points in a red region and *vice versa*. Nevertheless, the final picture given by DORIπ_{int} for the PTS is an overall higher π-overlap for the *Z*-configuration, which correspond to experimental findings.[93]

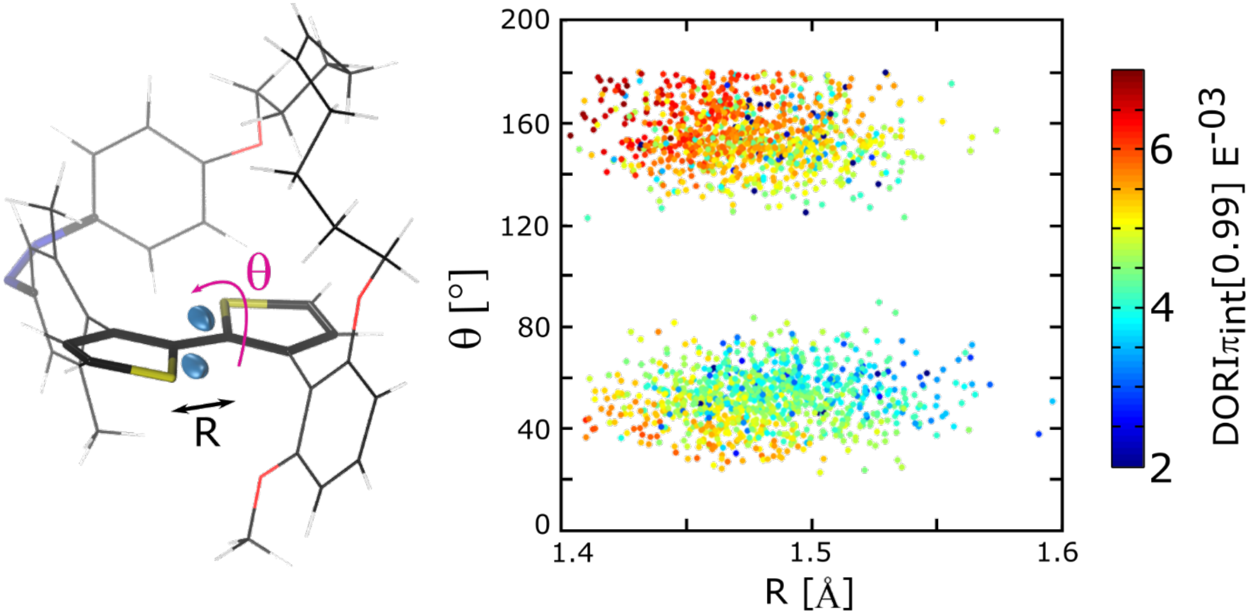

Figure 7: Representations of the photochromic torsional switch and its associated DORI$_{\pi int}$[0.99] (in blue, in electron/Bohr^3) for the inter-thiophene bond (left). Correlation of the DORIπ_{int}[0.99] with the inter-thiophene bond distance (R) and the inter-thiophene SCCS dihedral angle (θ), mapped in the [0,180] range. DORI are computed on electron densities relaxed at the PBE/6-31G* level on frozen DFTB3/3OB-UFF geometries from REMD.

Additional chemical insight is provided by comparing the DORI based sketch-map with its free-energy colored counterpart (Figure 8b). The later readily illustrates the highly-structured nature of *E*-azobenzene, which contrasts with the more disordered *Z*-configuration. The fact that DORI$_{\pi int}$ does not uncover this difference indicates that the overall flexibility of the molecule is not dominated by the bithiophene unit.

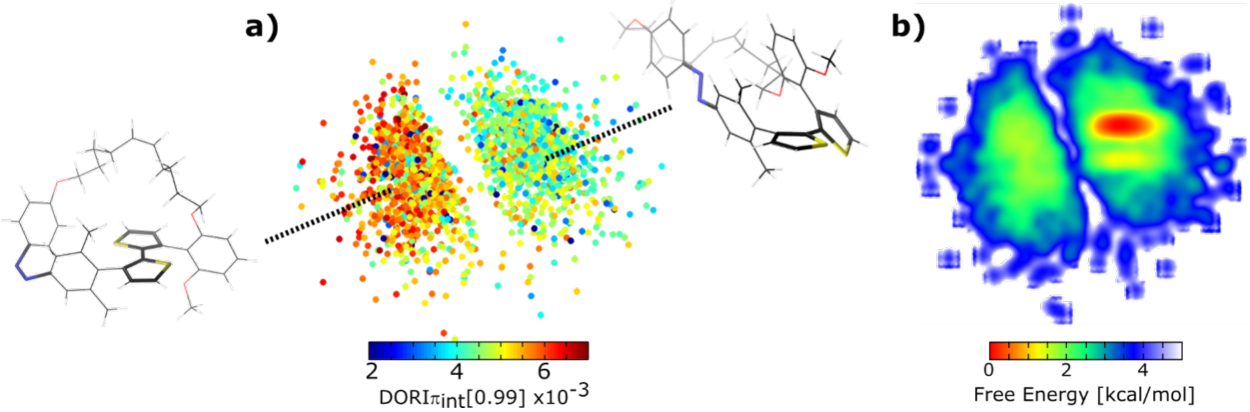

Figure 8: Sketch-map representation of the photochromic torsional switch **3**, producing two distinct zones corresponding to the Z- and E-azobenzene configuration (left and right respectively). The map is color-coded with the electron density integral stemming from the DORI$_{\pi}$ [0.99] (in electron/Bohr^3) domain of the dithiophene bridging bond (a), and with the free energy computed from the REMD occurrences (b).

Conclusion

In conclusion, we have shown that DORI provides unique insight into studies involving highly fluxional molecular systems. Using snapshots extracted from molecular dynamic simulations that exploited the efficiency of REMD@DFTB3, characteristic DORI-based electronic signatures were examined in tandem with a powerful data-driven low-dimensional representation of the structural landscapes. This procedure resulted in a picture that captured fluctuations arising from changes in bonding patterns and non-covalent interactions more clearly than with arbitrarily chosen geometrical collective variables. Thus, representations of complex conformational spaces and electronic processes can be described with no loss of structural information by using a single DORI-based variable.

The combination of DORI descriptors with sketch-map, a non-linear dimensionality reduction technique that strives to obtain a similarly general simplified description based on geometric parameters, cross-validates the two approaches. The strong correlation between the location of a configuration on a sketch-map and its corresponding DORI value (encoded with color) shows that DORI can distinguish structurally different conformations, and, vice versa, that sketch-map coordinates identify structural variables that are associated with marked changes in both covalent and non-covalent bonding. While, this work has focused on three illustrative systems characterized by specific fluctuating (non-)covalent interactions, similar analyses could be highly beneficial to better comprehend the massively different behavior types seen in chemistry and material sciences (*e.g.*, catalysis, supramolecular chemistry, amphidynamic crystals).

Acknowledgement

The Swiss NSF Grant 156001, the European Research Council (ERC starting Grants 306528, “COMPOREL”), and EPFL are gratefully acknowledged for their funding support. M. C. and C.C. acknowledge the National Centre of Competence in Research (NCCR) “Materials’ Revolution: Computational Design and Discovery of Novel Materials (MARVEL)”. L.V. thank Dr. Ganna Gryn’ova for insightful discussions. C.C. thank Dr. Piotr de Silva for his past contributions and discussions associated with DORI.

Supporting Information Available: Details on the dependence of the results on the computed DORI-based quantity and on the chosen isovalue; model systems used for the DORI computations, computational details on the Adaptative Natural Density Partitioning, specifications of the sketch-map parameters, $\mathrm{DORI}_{\mathrm{int}}$ for all MD trajectories, and Cartesian coordinates (in xyz.format) of the illustrative structures. This material is available free of charge via the Internet at http://pubs.acs.org.

References

(1) Anderson, J. S. M.; Melin, J.; Ayers, P. W. Conceptual Density-Functional Theory for General Chemical Reactions, Including Those That Are Neither Charge- nor Frontier-Orbital-Controlled. 1. Theory and Derivation of a General-Purpose Reactivity Indicator. *J. Chem. Theory Comput.* **2007**, *3*, 358–374.

(2) Gonthier, J. F.; Steinmann, S. N.; Wodrich, M. D.; Corminboeuf, C. Quantification of "fuzzy" Chemical Concepts: A Computational Perspective. *Chem. Soc. Rev.* **2012**, *41*, 4671–4687.

(3) Bultinck, P.; Van Alsenoy, C.; Ayers, P. W.; Carbó-Dorca, R. Critical Analysis and Extension of the Hirshfeld Atoms in Molecules. *J. Chem. Phys.* **2007**, *126*, 144111.

(4) Ayers, P. L.; Boyd, R. J.; Bultinck, P.; Caffarel, M.; Carbo-Dorca, R.; Causa, M.; Cioslowski, J.; Contreras-Garcia, J.; Cooper, D. L.; Coppens, P.; Gatti, C.; Grabowsky, S.; Lazzeretti, P.; Macchi, P.; Martin Pendas, A.; Popelier, P . L. A.; Ruedenberg, K.; Rzepa, H.; Savin, A.; Sax, A.; Schwarz, W. H. E.; Shahbazian, S.; Silvi, B.; Sola, M.; Tsirelson, V. Six Questions on Topology in Theoretical Chemistry. *Comput. Theor. Chem.* **2015**, *1053*, 2–16.

(5) Alvarez, S.; Hoffmann, R.; Mealli, C. A Bonding Quandary-or-A Demonstration of the Fact That Scientists Are Not Born With Logic. *Chem.—Eur. J.* **2009**, *15*, 8358–8373.

(6) Ball, P. Beyond the Bond. *Nature* **2011**, *469*, 26–28.

(7) von Schleyer, P. R.; Jiao, H. What Is Aromaticity? *Pure Appl. Chem.* **1996**, *68*, 209–218.

(8) Jansen, M.; Wedig, U. A Piece of the Picture-Misunderstanding of Chemical Concepts. *Angew. Chem., Int. Ed.* **2008**, *47*, 10026–10029.

(9) Becke, A. D.; Edgecombe, K. E. A Simple Measure of Electron Localization in Atomic and Molecular Systems. *J. Chem. Phys.* **1990**, *92*, 5397–5403.

(10) Savin, A.; Becke, A. D.; Flad, J.; Nesper, R.; Preuss, H.; von Schnering, H. G. A New Look at Electron Localization. *Angew. Chem., Int. Ed.* **1991**, *30*, 409–412.

(11) Silvi, B.; Savin, A. Classification of Chemical Bonds Based on Topological Analysis of Electron Localization Functions. *Nature* **1994**, *371*, 683–686.

(12) Schmider, H. .; Becke, A. . Chemical Content of the Kinetic Energy Density. *THEOCHEM* **2000**, *527*, 51–61.

(13) Schmider, H. A Parity Function for Studying the Molecular Electronic Structure. *J. Chem. Phys.* **1996**, *105*, 11134.

(14) Schmider, H. L.; Becke, A. D. Two Functions of the Density Matrix and Their Relation to the Chemical Bond. *J. Chem. Phys.* **2002**, *116*, 3184.

(15) Scemama, A.; Caffarel, M.; Chaudret, R.; Piquemal, J.-P. Electron Pair Localization Function (EPLF) for Density Functional Theory and Ab Initio Wave Function-Based Methods: A New Tool for Chemical Interpretation. *J. Chem. Theory Comput.* **2011**, *7*, 618–624.

(16) Bohórquez, H. J.; Boyd, R. J. A Localized Electrons Detector for Atomic and Molecular Systems. *Theor. Chem. Acc.* **2010**, *127*, 393–400.

(17) Kohout, M. A Measure of Electron Localizability. *Int. J. Quantum Chem.* **2004**, *97*, 651–658.

(18) Kohout, M.; Pernal, K.; Wagner, F. R.; Grin, Y. Electron Localizability Indicator for Correlated Wavefunctions. I. Parallel-Spin Pairs. *Theor. Chem. Acc.* **2004**, *112*, 453–459.

(19) Scemama, A.; Chaquin, P.; Caffarel, M. Electron Pair Localization Function: A Practical Tool to Visualize Electron Localization in Molecules from Quantum Monte Carlo Data. *J. Chem. Phys.* **2004**, *121*, 1725–1735.

(20) Johnson, E. R.; Keinan, S.; Mori-Sanchez, P.; Contreras-Garcia, J.; Cohen, A. J.; Yang, W. Revealing Noncovalent Interactions. *J. Am. Chem. Soc.* **2010**, *132*, 6498–6506.

(21) Gillet, N.; Chaudret, R.; Contreras-Garciia, J.; Yang, W.; Silvi, B.; Piquemal, J.-P. Coupling Quantum Interpretative Techniques: Another Look at Chemical Mechanisms in Organic Reactions. *J. Chem. Theory Comput.* **2012**, *8*, 3993–3997.

(22) Fang, D.; Chaudret, R.; Piquemal, J.-P.; Cisneros, G. A. Toward a Deeper Understanding of Enzyme Reactions Using the Coupled ELF/NCI Analysis: Application to DNA Repair Enzymes. *J. Chem. Theory Comput.* **2013**, *9*, 2156–2160.

(23) Popelier, P. On the Full Topology of the Laplacian of the Electron Density. *Coord. Chem. Rev.* **2000**, *197*, 169–189.

(24) Bader, R. F. W. In *Atoms in Molecules: A Quantum Theory*; Oxford Univer. Press, Oxford, 1990.

(25) Bader, R. F. W.; Gillespie, R. J.; MacDougall, P. J. A Physical Basis for the VSEPR Model of Molecular Geometry. *J. Am. Chem. Soc.* **1988**, *110*, 7329–7336.

(26) Bader, R. F. W.; Essén, H. The Characterization of Atomic Interactions. *J. Chem. Phys.* **1984**, *80*, 1943–1960.

(27) de Silva, P.; Corminboeuf, C. Simultaneous Visualization of Covalent and Noncovalent Interactions Using Regions of Density Overlap. *J. Chem. Theory Comput.* **2014**, *10*, 3745–3756.

(28) de Silva, P.; Korchowiec, J.; Wesolowski, T. A. Revealing the Bonding Pattern from the Molecular Electron Density Using Single Exponential Decay Detector: An Orbital-Free Alternative to the Electron Localization Function. *ChemPhysChem* **2012**, *13*, 3462–3465.

(29) de Silva, P.; Korchowiec, J.; Ram J. S., N.; Wesolowski, T. A. Extracting Information about Chemical Bonding from Molecular Electron Densities via Single Exponential Decay Detector (SEDD). *Chimia* **2013**, *67*, 253–256.

(30) de Silva, P.; Korchowiec, J.; Wesolowski, T. A. Atomic Shell Structure from the Single-Exponential Decay Detector. *J. Chem. Phys.* **2014**, *140*, 164301.

(31) Vannay, L.; Meyer, B.; Guillot, B.; Corminboeuf, C. The Interplay between Covalent bonding Patterns and Non-Covalent Interactions in Biscarbonyl[14] Annulene under Pressure. *In Preparation*.

(32) Nagy, Á.; Liu, S. Local Wave-Vector, Shannon and Fisher Information. *Phys. Lett. A* **2008**, *372*, 1654–1656.

(33) Bohórquez, H. J.; Boyd, R. J. On the Local Representation of the Electronic Momentum Operator in Atomic Systems. *J. Chem. Phys.* **2008**, *129*, 24110.

(34) Nagy, A.; March, N. H. Ratio of Density Gradient to Electron Density as a Local Wavenumber to Characterize the Ground State of Spherical Atoms. *Mol. Phys.* **1997**, *90*, 271–276.

(35) Poater, J.; Duran, M.; Solà, M.; Silvi, B. Theoretical Evaluation of Electron Delocalization in Aromatic Molecules by Means of Atoms in Molecules (AIM) and Electron Localization Function (ELF) Topological Approaches. *Chem. Rev.* **2005**, *105*, 3911–3947.

(36) Feixas, F.; Matito, E.; Poater, J.; Solà, M. Quantifying Aromaticity with Electron Delocalisation Measures. *Chem. Soc. Rev.* **2015**, *44*, 6434–6451.

(37) Tiana, D.; Francisco, E.; Macchi, P.; Sironi, A.; Martín Pendás, A. An Interacting Quantum Atoms Analysis of the Metal–Metal Bond in $[M_2\,(CO)_8]^n$ Systems. *J. Phys. Chem. A* **2015**, *119*, 2153–2160.

(38) Butovskii, M. V; Döring, C.; Bezugly, V.; Wagner, F. R.; Grin, Y.; Kempe, R. Molecules

Containing Rare-Earth Atoms Solely Bonded by Transition Metals. *Nat. Chem.* **2010**, *2*, 741–744.

(39) Vidal, I.; Melchor, S.; Dobado, J. A. On the Nature of Metal−Carbon Bonding: AIM and ELF Analyses of MCH N (N = 1−3) Compounds Containing Early Transition Metals. *J. Phys. Chem. A* **2005**, *109*, 7500–7508.

(40) Tiana, D.; Francisco, E.; Blanco, M. A.; Macchi, P.; Sironi, A.; Martin Pendas, A. Bonding in Classical and Nonclassical Transition Metal Carbonyls: The Interacting Quantum Atoms Perspective. *J. Chem. Theory Comput.* **2010**, *6*, 1064–1074.

(41) Sánchez-Sanz, G.; Trujillo, C.; Solimannejad, M.; Alkorta, I.; Elguero, J. Orthogonal Interactions between Nitryl Derivatives and Electron Donors: Pnictogen Bonds. *Phys. Chem. Chem. Phys.* **2013**, *15*, 14310–14318.

(42) Bader, R. F. W.; Johnson, S.; Tang, T.-H.; Popelier, P. L. A. The Electron Pair. *J. Phys. Chem.* **1996**, *100*, 15398–15415.

(43) Fradera, X.; Austen, M. A.; Bader, R. F. W. The Lewis Model and Beyond. *J. Phys. Chem. A* **1999**, *103*, 304–314.

(44) Cortesguzman, F.; Bader, R. Complementarity of QTAIM and MO Theory in the Study of Bonding in Donor-Acceptor Complexes. *Coord. Chem. Rev.* **2005**, *249*, 633–662.

(45) Mebs, S. Complex Modes of Bonding: NCI/ELI-D vs. DORI Surface Analyses of Hapticities and Hydrogen–hydrogen Contacts in Zincocene Related Compounds. *Chem. Phys. Lett.* **2016**, *651*, 172–177.

(46) Cormanich, R. A.; Bühl, M.; Rittner, R. Understanding the Conformational Behaviour of Ac-Ala-NHMe in Different Media. A Joint NMR and DFT Study. *Org. Biomol. Chem.* **2015**, *13*, 9206–9213.

(47) Causà, M.; Savin, A. Maximum Probability Domains in Crystals: The Rock-Salt Structure. *J. Phys. Chem. A* **2011**, *115*, 13139–13148.

(48) Fourré, I.; Silvi, B. What Can We Learn from Two-Center Three-Electron Bonding with the Topological Analysis of ELF? *Heteroat. Chem.* **2007**, *18*, 135–160.

(49) Fuster, F.; Silvi, B. Does the Topological Approach Characterize the Hydrogen Bond? *Theor. Chim. Acta* **2000**, *104*, 13–21.

(50) Fuster, F.; Grabowski, S. J. Intramolecular Hydrogen Bonds: The QTAIM and ELF Characteristics. *J. Phys. Chem. A* **2011**, *115*, 10078–10086.

(51) Contreras-Garcia, J.; Yang, W.; Johnson, E. R. Analysis of Hydrogen-Bond Interaction Potentials from the Electron Density: Integration of Noncovalent Interaction Regions. *J. Phys. Chem. A* **2011**, *115*, 12983–12990.

(52) Amezaga, N. J. M.; Pamies, S. C.; Peruchena, N. M.; Sosa, G. L. Halogen Bonding: A Study Based on the Electronic Charge Density. *J. Phys. Chem. A* **2010**, *114*, 552–562.

(53) Syzgantseva, O. A.; Tognetti, V.; Joubert, L. On the Physical Nature of Halogen Bonds: A QTAIM Study. *J. Phys. Chem. A* **2013**, *117*, 8969–8980.

(54) Bartashevich, E. V; Pendas, A. M.; Tsirelson, V. G. An Anatomy of Intramolecular Atomic Interactions in Halogen-Substituted Trinitromethanes. *Phys. Chem. Chem. Phys.* **2014**, *16*, 16780–16789.

(55) Johansson, M. P.; Swart, M. Intramolecular Halogen–halogen Bonds? *Phys. Chem. Chem. Phys.* **2013**, *15*, 11543–11553.

(56) Polo, V.; Andres, J.; Castillo, R.; Berski, S.; Silvi, B. Understanding the Molecular Mechanism of the 1,3-Dipolar Cycloaddition between Fulminic Acid and Acetylene in Terms of the Electron Localization Function and Catastrophe Theory. *Chem.—Eur. J.* **2004**,

10, 5165–5172.

(57) Berski, S.; Latajka, Z. Quantum Chemical Topology Description of the Hydrogen Transfer between the Ethynyl Radical and Ammonia (C2H+NH3) – The Electron Localization Function Study. *Chem. Phys. Lett.* **2006**, *426*, 273–279.

(58) Kalinowski, J.; Berski, S.; Gordon, A. J. Electron Localization Function Study on Intramolecular Electron Transfer in the QTTFQ and DBTTFI Radical Anions. *J. Phys. Chem. A* **2011**, *115*, 13513–13522.

(59) Lee, R.; Gryn'ova, G.; Ingold, K. U.; Coote, M. L. Why Are Sec-Alkylperoxyl Bimolecular Self-Reactions Orders of Magnitude Faster than the Analogous Reactions of Tert-Alkylperoxyls? The Unanticipated Role of CH Hydrogen Bond Donation. *Phys. Chem. Chem. Phys.* **2016**, *18*, 23673–23679.

(60) Polo, V.; Andres, J.; Berski, S.; Domingo, L. R.; Silvi, B. Understanding Reaction Mechanisms in Organic Chemistry from Catastrophe Theory Applied to the Electron Localization Function Topology. *J. Phys. Chem. A* **2008**, *112*, 7128–7136.

(61) Berski, S.; Andrés, J.; Silvi, B.; Domingo, L. R. New Findings on the Diels−Alder Reactions. An Analysis Based on the Bonding Evolution Theory. *J. Phys. Chem. A* **2006**, *110*, 13939–13947.

(62) Chaudry, U. A.; Popelier, P. L. A. Ester Hydrolysis Rate Constant Prediction from Quantum Topological Molecular Similarity Descriptors. *J. Phys. Chem. A* **2003**, *107*, 4578–4582.

(63) Andrés, J.; Gracia, L.; González-Navarrete, P.; Safont, V. S. Chemical Structure and Reactivity by Means of Quantum Chemical Topology Analysis. *Comput. Theor. Chem.* **2015**, *1053*, 17–30.

(64) Chattaraj, P. K.; Roy, D. R.; Elango, M.; Subramanian, V. Stability and Reactivity of All-Metal Aromatic and Antiaromatic Systems in Light of the Principles of Maximum Hardness and Minimum Polarizability. *J. Phys. Chem. A* **2005**, *109*, 9590–9597.

(65) de Silva, P.; Corminboeuf, C. Local Hybrid Functionals with Orbital-Free Mixing Functions and Balanced Elimination of Self-Interaction Error. *J. Chem. Phys.* **2015**, *142*, 74112.

(66) de Silva, P.; Corminboeuf, C. Communication: A New Class of Non-Empirical Explicit Density Functionals on the Third Rung of Jacob's Ladder. *J. Chem. Phys.* **2015**, *143*, 111105.

(67) Zheng, M.; Kuriappan, J. A.; Waller, M. P. Toward More Efficient Density-Based Adaptive QM/MM Methods. *Int. J. Quantum Chem.* **2017**, *117*, e25336.

(68) Nicolaï, A.; Liu, H.; Petraglia, R.; Corminboeuf, C. Exploiting Dispersion-Driven Aggregators as a Route to New One-Dimensional Organic Nanowires. *J. Phys. Chem. Lett.* **2015**, *6*, 4422–4428.

(69) Vannay, L.; Brémond, E.; de Silva, P.; Corminboeuf, C. Visualizing and Quantifying Interactions in the Excited State. *Chem.—Eur. J.* **2016**, *22*, 18442–18449.

(70) Prlj, A.; Vannay, L.; Corminboeuf, C. Fluorescence Quenching in BODIPY Dyes: The Role of Intramolecular Interactions and Charge Transfer. *Helv. Chim. Acta* **2017**, *100*, e1700093.

(71) de Lima Batista, A. P.; de Oliveira-Filho, A. G. S.; Galembeck, S. E. CO 2 Sequestration by Triazolylidene-Derived N-Heterocyclic Olefins: A Computational Study. *ChemistrySelect* **2017**, *2*, 4648–4654.

(72) Bürgi, T.; Baiker, A. Conformational Behavior of Cinchonidine in Different Solvents: A Combined NMR and Ab Initio Investigation. *J. Am. Chem. Soc.* **1998**, *120*, 12920–12926.

(73) Koumura, N.; Zijlstra, R. W. J.; van Delden, R. A.; Harada, N.; Feringa, B. L. Light-Driven Monodirectional Molecular Rotor. *Nature* **1999**, *401*, 152–155.

(74) Ashton, P. R.; Ballardini, R.; Balzani, V. V; Credi, A.; Dress, K. R.; Ishow, E.; Kleverlaan, C. J.; Kocian, O.; Preece, J. A.; Spencer, N.; Stoddart, J. F.; Venturi, M.; Wenger, S. A Photochemically Driven Molecular-Level Abacus. *Chem.—Eur. J.* **2000**, *6*, 3558–3574.
(75) Shin, J.-S.; Pierce, N. A. A Synthetic DNA Walker for Molecular Transport. *J. Am. Chem. Soc.* **2004**, *126*, 10834–10835.
(76) Holland, N. B.; Hugel, T.; Neuert, G.; Cattani-Scholz, A.; Renner, C.; Oesterhelt, D.; Moroder, L.; Seitz, M.; Gaub, H. E. Single Molecule Force Spectroscopy of Azobenzene Polymers: Switching Elasticity of Single Photochromic Macromolecules. *Macromolecules* **2003**, *36*, 2015–2023.
(77) Russew, M.-M.; Hecht, S. Photoswitches: From Molecules to Materials. *Adv. Mater.* **2010**, *22*, 3348–3360.
(78) Beharry, A. A.; Woolley, G. A. Azobenzene Photoswitches for Biomolecules. *Chem. Soc. Rev.* **2011**, *40*, 4422–4437.
(79) Tian, H.; Yang, S. Recent Progresses on Diarylethene Based Photochromic Switches. *Chem. Soc. Rev.* **2004**, *33*, 85–97.
(80) Gryn'ova, G.; Nicolaï, A.; Prlj, A.; Ollitrault, P.; Andrienko, D.; Corminboeuf, C. Charge Transport in Highly Ordered Organic Nanofibrils: Lessons from Modelling. *J. Mater. Chem. C* **2017**, *5*, 350–361.
(81) Krokidis, X.; Noury, S.; Silvi, B. Characterization of Elementary Chemical Processes by Catastrophe Theory. *J. Phys. Chem. A* **1997**, *101*, 7277–7282.
(82) Krokidis, X.; Silvi, B.; Alikhani, M. E. Topological Characterization of the Isomerization Mechanisms in XNO (X=H, Cl). *Chem. Phys. Lett.* **1998**, *292*, 35–45.
(83) Thom, R. Catastrophe Theory. *Nature* **1977**, *270*, 658.
(84) Andres, J.; Berski, S.; R. Domingo, L.; Polo, V.; Silvi, B. Describing the Molecular Mechanism of Organic Reactions by Using Topological Analysis of Electronic Localization Function. *Curr. Org. Chem.* **2011**, *15*, 3566–3575.
(85) Andrés, J.; González-Navarrete, P.; Safont, V. S. Unraveling Reaction Mechanisms by Means of Quantum Chemical Topology Analysis. *Int. J. Quantum Chem.* **2014**, *114*, 1239–1252.
(86) Wu, P.; Chaudret, R.; Hu, X.; Yang, W. Noncovalent Interaction Analysis in Fluctuating Environments. *J. Chem. Theory Comput.* **2013**, *9*, 2226–2234.
(87) Joubert, L.; Pavone, M.; Barone, V.; Adamo, C. Comparative Static and Dynamic Study of a Prototype S N 2 Reaction. *J. Chem. Theory Comput.* **2006**, *2*, 1220–1227.
(88) Marx, D.; Savin, A. Topological Bifurcation Analysis: Electronic Structure of CH5+. *Angew. Chem., Int. Ed.* **1997**, *36*, 2077–2080.
(89) Mashraqui, S. H.; Sangvikar, Y. S.; Meetsma, A. Synthesis and Structures of thieno[2,3-B]thiophene Incorporated [3.3]dithiacyclophanes. Enhanced First Hyperpolarizability in an Unsymmetrically Polarized Cyclophane. *Tetrahedron Lett.* **2006**, *47*, 5599–5602.
(90) Brémond, É.; Golubev, N.; Steinmann, S. N.; Corminboeuf, C. How Important Is Self-Consistency for the dDsC Density Dependent Dispersion Correction? *J. Chem. Phys.* **2014**, *140*, 18A516.
(91) Petraglia, R.; Nicolaï, A.; Wodrich, M. D.; Ceriotti, M.; Corminboeuf, C. Beyond Static Structures: Putting Forth REMD as a Tool to Solve Problems in Computational Organic Chemistry. *J. Comput. Chem.* **2016**, *37*, 83–92.
(92) Perez-Estrada, S.; Rodriguez-Molina, B.; Xiao, L.; Santillan, R.; Jimenez-Oses, G.; Houk, K. N.; Garcia-Garibay, M. A. Thermodynamic Evaluation of Aromatic CH/π Interactions

and Rotational Entropy in a Molecular Rotor. *J. Am. Chem. Soc.* **2015**, *137*, 2175–2178.

(93) Maciejewski, J.; Sobczuk, A.; Claveau, A.; Nicolai, A.; Petraglia, R.; Cervini, L.; Baudat, E.; Miéville, P.; Fazzi, D.; Corminboeuf, C.; Sforazzini, G. Photochromic Torsional Switch (PTS): A Light-Driven Actuator for the Dynamic Tuning of π-Conjugation Extension. *Chem. Sci.* **2017**, *8*, 361–365.

(94) Elstner, M.; Porezag, D.; Jungnickel, G.; Elsner, J.; Haugk, M.; Frauenheim, T.; Suhai, S.; Seifert, G. Self-Consistent-Charge Density-Functional Tight-Binding Method for Simulations of Complex Materials Properties. *Phys. Rev. B* **1998**, *58*, 7260–7268.

(95) Porezag, D.; Frauenheim, T.; Köhler, T.; Seifert, G.; Kaschner, R. Construction of Tight-Binding-like Potentials on the Basis of Density-Functional Theory: Application to Carbon. *Phys. Rev. B* **1995**, *51*, 12947–12957.

(96) Yang; Yu, H.; York, D.; Cui, Q.; Elstner, M. Extension of the Self-Consistent-Charge Density-Functional Tight-Binding Method: Third-Order Expansion of the Density Functional Theory Total Energy and Introduction of a Modified Effective Coulomb Interaction. *J. Phys. Chem. A* **2007**, *111*, 10861–10873.

(97) Aradi, B.; Hourahine, B.; Frauenheim, T. DFTB+, a Sparse Matrix-Based Implementation of the DFTB Method. *J. Phys. Chem. A* **2007**, *111*, 5678–5684.

(98) Sugita, Y.; Okamoto, Y. Replica-Exchange Molecular Dynamics Method for Protein Folding. *Chem. Phys. Lett.* **1999**, *314*, 141–151.

(99) Ceriotti, M.; More, J.; Manolopoulos, D. E. I-PI: A Python Interface for Ab Initio Path Integral Molecular Dynamics Simulations. *Comput. Phys. Commun.* **2014**, *185*, 1019–1026.

(100) Ceriotti, M.; Bussi, G.; Parrinello, M. Colored-Noise Thermostats À La Carte. *J. Chem. Theory Comput.* **2010**, *6*, 1170–1180.

(101) Gaus, M.; Lu, X.; Elstner, M.; Cui, Q. Parameterization of DFTB3/3OB for Sulfur and Phosphorus for Chemical and Biological Applications. *J. Chem. Theory Comput.* **2014**, *10*, 1518–1537.

(102) Gaus, M.; Goez, A.; Elstner, M. Parametrization and Benchmark of DFTB3 for Organic Molecules. *J. Chem. Theory Comput.* **2013**, *9*, 338–354.

(103) Dolgonos, G.; Aradi, B.; Moreira, N. H.; Frauenheim, T. An Improved Self-Consistent-Charge Density-Functional Tight-Binding (SCC-DFTB) Set of Parameters for Simulation of Bulk and Molecular Systems Involving Titanium. *J. Chem. Theory Comput.* **2010**, *6*, 266–278.

(104) Zubarev, D. Y.; Boldyrev, A. I. Developing Paradigms of Chemical Bonding: Adaptive Natural Density Partitioning. *Phys. Chem. Chem. Phys.* **2008**, *10*, 5207.

(105) Foster, J. P.; Weinhold, F. Natural Hybrid Orbitals. *J. Am. Chem. Soc.* **1980**, *102*, 7211–7218.

(106) Zubarev, D. Y.; Boldyrev, A. I. Revealing Intuitively Assessable Chemical Bonding Patterns in Organic Aromatic Molecules via Adaptive Natural Density Partitioning. *J. Org. Chem.* **2008**, *73*, 9251–9258.

(107) Ceriotti, M.; Tribello, G. A.; Parrinello, M. Simplifying the Representation of Complex Free-Energy Landscapes Using Sketch-Map. *Proc. Natl. Acad. Sci. U.S.A.* **2011**, *108*, 13023–13028.

(108) Ceriotti, M.; Tribello, G. A.; Parrinello, M. Demonstrating the Transferability and the Descriptive Power of Sketch-Map. *J. Chem. Theory Comput.* **2013**, *9*, 1521–1532.

(109) Tribello, G. A.; Ceriotti, M.; Parrinello, M. Using Sketch-Map Coordinates to Analyze and Bias Molecular Dynamics Simulations. *Proc. Natl. Acad. Sci. U.S.A.* **2012**, *109*, 5196–5201.

(110) Bashir, A.; Heck, A.; Narita, A.; Feng, X.; Nefedov, A.; Rohwerder, M.; Müllen, K.; Elstner, M.; Wöll, C. Charge Carrier Mobilities in Organic Semiconductors: Crystal Engineering and the Importance of Molecular Contacts. *Phys. Chem. Chem. Phys.* **2015**, *17*, 21988–21996.

(111) Gleiter Rolf, H. H. In *Modern Cyclophane Chemistry*; Gleiter, R., Hopf, H., Eds.; Wiley-VCH, Weinheim, 2004.

(112) Garcia-Garibay, M. A. Crystalline Molecular Machines: Encoding Supramolecular Dynamics into Molecular Structure. *Proc. Natl. Acad. Sci. U.S.A.* **2005**, *102*, 10771–10776.

(113) Nawara, A. J.; Shima, T.; Hampel, F.; Gladysz, J. A. Gyroscope-like Molecules Consisting of PdX 2 /PtX 2 Rotators Encased in Three-Spoke Stators: Synthesis via Alkene Metathesis, and Facile Substitution and Demetalation. *J. Am. Chem. Soc.* **2006**, *128* , 4962–4963.

(114) Hawthorne, M. F. Electrical or Photocontrol of the Rotary Motion of a Metallacarborane. *Science* **2004**, *303*, 1849–1851.

(115) Rapenne, G. Synthesis of Technomimetic Molecules: Towards Rotation Control in Single-Molecular Machines and Motors. *Org. Biomol. Chem.* **2005**, *3*, 1165–1169.

(116) Kottas, G. S.; Clarke, L. I.; Horinek, D.; Michl, J. Artificial Molecular Rotors. *Chem. Rev.* **2005**, *105*, 1281–1376.

(117) Wold, S.; Esbensen, K.; Geladi, P. Principal Component Analysis. *Chemom. Intell. Lab. Syst.* **1987**, *2*, 37–52.

(118) Sittel, F.; Jain, A.; Stock, G. Principal Component Analysis of Molecular Dynamics: On the Use of Cartesian vs. Internal Coordinates. *J. Chem. Phys.* **2014**, *141*, 14111.

(119) Garcia, A. E. Large-Amplitude Nonlinear Motions in Proteins. *Phys. Rev. Lett.* **1992**, *68*, 2696–2699.

(120) Tenenbaum, J. B. A Global Geometric Framework for Nonlinear Dimensionality Reduction. *Science* **2000**, *290* , 2319–2323.

(121) Belkin, M.; Niyogi, P. Laplacian Eigenmaps for Dimensionality Reduction and Data Representation. *Neural Comput.* **2003**, *15*, 1373–1396.

(122) Roweis, S. T. Nonlinear Dimensionality Reduction by Locally Linear Embedding. *Science* **2000**, *290*, 2323–2326.

(123) Ardevol, A.; Tribello, G. A.; Ceriotti, M.; Parrinello, M. Probing the Unfolded Configurations of a β-Hairpin Using Sketch-Map. *J. Chem. Theory Comput.* **2015**, *11*, 1086–1093.

(124) De, S.; Bartók, A. P.; Csányi, G.; Ceriotti, M. Comparing Molecules and Solids across Structural and Alchemical Space. *Phys. Chem. Chem. Phys.* **2016**, *18*, 13754–13769.

(125) De, S.; Musil, F.; Ingram, T.; Baldauf, C.; Ceriotti, M. Mapping and Classifying Molecules from a High-Throughput Structural Database. *J. Cheminform.* **2017**, *9*, 6.

TOC Graphic: